MCB
Journals.ASM.org

Structure and Dimerization Properties of the Aryl Hydrocarbon Receptor PAS-A Domain

Dalei Wu,[a] Nalini Potluri,[a] Youngchang Kim,[b] Fraydoon Rastinejad[a]

Metabolic Signaling and Disease Program, Sanford-Burnham Medical Research Institute, Orlando, Florida, USA[a]; Biosciences Division, Structure Biology Center, Argonne National Laboratory, Argonne, Illinois, USA[b]

The aryl hydrocarbon receptor (AHR) is a ligand-dependent transcription factor that binds to xenobiotics and responds by regulating the expression of gene programs required for detoxification and metabolism. AHR and its heterodimerization partner aryl hydrocarbon receptor nuclear translocator (ARNT) belong to the basic helix-loop-helix (bHLH)–PER-ARNT-SIM (PAS) family of transcription factors. Here we report the 2.55-Å-resolution crystal structure of the mouse AHR PAS-A domain, which represents the first AHR-derived protein structure. The AHR PAS-A domain forms a helix-swapped homodimer in the crystal and also in solution. Through a detailed mutational analysis of all interface residues, we identified several hydrophobic residues that are important for AHR dimerization and function. Our crystallographic visualization of AHR PAS-A dimerization leads us to propose a mode of heterodimerization with ARNT that is supported by both biochemical and cell-based data. Our studies also highlight the residues of other mammalian bHLH-PAS proteins that are likely involved in their homo- or heterodimerization.

The PER-ARNT-SIM (PAS) domains, originally identified by sequence homology in the *Drosophila melanogaster* proteins period and single-minded (encoded by the genes *per* and *sim*, respectively), as well as the vertebrate protein aryl hydrocarbon receptor nuclear translocator (ARNT), are conserved motifs that function as sensors and interaction modules in a variety of proteins (1, 2). A subgroup of PAS domain proteins belong to the basic helix-loop-helix (bHLH) family (3). These bHLH-PAS transcription factors usually contain the bHLH DNA binding domain (also involved in dimerization) at their N-terminal regions and tandemly positioned PAS domains (PAS-A and PAS-B), followed by a transactivation or transrepression domain at their C-terminal regions (3). The aryl hydrocarbon receptor (AHR) and ARNT are both members of this family. In AHR, both PAS domains are used for heterodimerization with ARNT; meanwhile, the PAS-B domain also serves as the ligand binding domain (LBD) (4).

Since the 1970s, AHR has been known to be a mediator for the toxicities of environmental pollutants, including 2,3,7,8-tetrachlorodibenzo-*p*-dioxin (TCDD). The ligand-bound AHR:ARNT heterodimer recognizes and initiates transcription from xenobiotic response elements (XREs) of target genes typified by the xenobiotic metabolizing enzymes like cytochrome P450 1A1 (3). Another target gene encodes the bHLH-PAS protein aryl hydrocarbon receptor repressor (AHRR) (5), which represses the transcriptional activity of AHR by heterodimerizing with ARNT and binding to the XRE. Some intrinsic physiological roles of AHR have also been revealed by recent studies. For example, AHR can function as a ligand-dependent E3 ubiquitin ligase targeting sex steroid receptors (6), control regulatory T (T_{reg}) and interleukin 17 (IL-17)-producing T (T_H17) cell differentiation (7, 8), promote tumor cell survival and motility when activated by the endogenous ligand kynurenine (9), maintain intraepithelial lymphocyte (IEL) numbers (10), and regulate organogenesis of intestinal lymphoid follicles (11).

Based on the choice of dimerization partners, the bHLH-PAS proteins have been divided into two classes (2, 3). Class I (class α) members can form heterodimers only with a class II (class β) protein, while class II members can promiscuously form homodimers or can form heterodimers with a partner from class I. Aside from AHR and AHRR, other mammalian class I members involved in different functions are three hypoxia-inducible factors (HIF-1α, HIF-2α, and HIF-3α), which activate the transcription of target genes critical for survival under low-oxygen conditions (2, 3); SIM1 and SIM2, homologues of the *Drosophila* protein single-minded, which function as transcriptional repressors in embryogenesis (12); CLOCK and its paralog NPAS2 (neuronal PAS domain protein 2), the major transcriptional regulators of circadian rhythm (2, 13); NPAS1, which acts as a transcriptional repressor by dimerizing with ARNT or ARNT2 and functions in neuronal differentiation (14); NPAS3, a potential repressor which downregulates multiple hypoxia-related genes when overexpressed in HEK 293 cells (15); and NPAS4, an activity-dependent transcription factor required for contextual memory formation (16). Mammalian class II bHLH-PAS proteins include ARNT, ARNT2, BMAL1 (brain and muscle ARNT-like protein 1, also known as ARNTL1), and BMAL2 (ARNTL2).

The first characterized mammalian bHLH-PAS protein architectures were the PAS-B domains derived from human HIF-2α (17) and ARNT (18). Those studies revealed a β-sheet interface used for PAS-B dimerization. The structure determinate of the HIF-2α:ARNT PAS-B complex confirmed this dimerization surface and further revealed how the HIF-2α PAS-B domain binds to synthetic small-molecule ligands that modulate the dimerization of the heterodimer (19, 20). More recently, the crystal structure of the mouse CLOCK:BMAL1 complex illustrated the multifaceted interactions between the bHLH, PAS-A, and PAS-B domains (21). However, only one residue from PAS-A domains (Ile317 of

Received 4 June 2013 Returned for modification 24 June 2013
Accepted 27 August 2013
Published ahead of print 3 September 2013
Address correspondence to Fraydoon Rastinejad, frastinejad@sanfordburnham.org.

doi:10.1128/MCB.00698-13

BMAL1) was identified to be critical for the heterodimerization and transactivation function of this complex (21).

Besides the CLOCK:BMAL1 complex, no other mammalian bHLH-PAS heterodimeric structures are available to suggest how the AHR:ARNT heterodimer may be forming its intermolecular interactions through the PAS domains. Hao et al. identified several residues used for dimerization in the PAS-A domains of ARNT and AHR through a two-hybrid approach (22), finding that ARNT and AHR interact through equivalent regions of their PAS-A domains. To date, no structure has been available for any AHR protein segment, despite the intense interest in the physiological functions of this transcription factor. Here, we present the crystal structure of the AHR PAS-A domain and through a combination of solution- and cell-based studies further reveal the basis for reciprocal AHR:ARNT heterodimerization interactions through their PAS-A domains.

MATERIALS AND METHODS

Plasmid construction and site-directed mutagenesis. For the overexpression of the mouse AHR (mAHR) PAS-A domain protein with a 6×His tag in *Escherichia coli*, a DNA fragment encoding residues 110 to 267 (mAHR 110–267) was cloned into the vector pSJ2 (derived from pET, a generous gift from Jian Wu at the University of Michigan). A similar strategy was applied to the cloning of mAHR residues 7 to 267 (mAHR 7–267) into pSJ2 and a fragment encoding mouse ARNT residues 82 to 346 (mARNT 82–346) into pMKH (no tag; a gift from Weizhi Liu at Yale University). For the transactivation assays and coimmunoprecipitation (co-IP) experiments, full-length mAHR and mARNT were cloned into the pCMV-Tag4 and pCMV-Tag1 vectors with a C-terminal Flag tag and Myc tag, respectively. Site-directed mutagenesis for both mAHR and mARNT was performed as described previously (23) and confirmed by DNA sequencing. To generate the deletion mutant ΔA′α (Δ110-119), mAHR DNA was PCR amplified as two fragments (with the first fragment ending at Gln108 and the second starting at Asn121), digested, and ligated together through the HindIII site (AAGCTT), which was positioned on both fragments and finally mutated to GATCTT to encode Asp109 and Leu120.

Protein expression, purification, and crystallization. The recombinant plasmid pSJ2-mAHR 110-267 was transformed into BL21-CodonPlus (DE3)-RIL competent cells (Agilent Technologies) for expression. After purification by His·Bind resin (Novagen), the protein sample was concentrated and loaded on a Superdex 200pg (GE Healthcare) gel filtration column using 20 mM Tris (pH 8.0)–150 mM NaCl as the running buffer. Protein crystals of mAHR 110-267 were grown at 4°C in sitting drops equilibrated versus the reservoir solution, which consisted of 100 mM HEPES (pH 7.5), 1.6 M $(NH_4)_2SO_4$, and 2% polyethylene glycol (PEG) 1000. Crystals reached the maximum size about 3 months after setup and were soaked in cryoprotectant solution containing 30% glycerol before flash freezing in liquid nitrogen.

X-ray data collection, structure determination and refinement. Diffraction data were collected at the Argonne National Laboratory SBC-CAT 19ID beamline at a single wavelength of 0.9793 Å at 100 K and diffracted up to 2.55 Å. The data set was indexed and processed using the HKL3000 software program (24). The structure was solved by molecular replacement (MR) using the program Phaser (25) in the CCP4 (26) program suite 6.2.0, using PAS-A domain structures from three coordinates, 2VLG (27), 3RTY (28), and 3GEC (29), as the combined search model. Further model building was facilitated by using Coot (30), and structure refinement was performed using the programs Refmac5 (31) and phenix.refine (32). Residues 180 to 205 and 245 to 252 are disordered with no visible electron density map in chain A, as are residues 177 to 206, 223 to 226, and 240 to 253 in chain B. All the structural figures were prepared using the software program PyMOL (PyMOL Molecular Graphics System, version 1.3; Schrödinger, LLC).

Gel filtration chromatography. After purification by using His·Bind resin, 2.5 ml of mAHR 110–267 (wild type [WT], ΔA′α, or other point mutants) protein samples were loaded on the Superdex 200pg gel filtration column using 20 mM Tris (pH 8.0)–150 mM NaCl as the running buffer at 1.5 ml/min. The concentrations of injected samples were 8 to 120 μM for the WT, 120 μM for the ΔA′α mutant, and about 80 μM for the other point mutants. The marker proteins albumin (66 kDa), carbonic anhydrase (29 kDa), and cytochrome *c* (12.4 kDa) were dissolved in 2.5 ml running buffer and injected into the column in the same way to serve as calibration standards.

Ni affinity pulldown. The recombinant plasmid pSJ2-mAHR 7-267 (WT or ΔA′α) was transformed alone or cotransformed with pMKH-mARNT 82-346 into BL21 *E. coli* cells. After sonication and high-speed spinning, the cell lysate was loaded onto His·Bind resin, washed with buffer containing 30 mM imidazole, and then eluted with 300 mM imidazole buffer. The elution samples were finally analyzed by SDS-PAGE and gel staining.

Transactivation assay (XRE luciferase reporter assay). Murine hepatoma Tao cells and HEK 293T cells were grown in minimal essential medium (MEM) alpha and Dulbecco's modified Eagle medium (DMEM) supplemented with 10% fetal bovine serum (FBS) and 1% penicillin-streptomycin (Gibco, Life Technologies), respectively. For the luciferase assay testing the AHR WT and mutants, cells were seeded in 24-well plates and 1 day later transfected with 200 ng of pCMV-Tag4-mAHR (full-length WT, mutants, or empty plasmid), 400 ng of XRE reporter (containing the XRE1 sequence of the rat *Cyp1a1* gene promoter region −1029 to −997), and 5 ng of pRL (control *Renilla* luciferase) using 1.2 μl jetPEI reagent (Polyplus transfection) for each well according to the manufacturer's protocol. For the luciferase assay testing the ARNT WT and mutants, 293T cells were seeded in the same way and cotransfected with 100 ng of pCMV-Tag4-mAHR WT, 250 ng of pCMV-Tag1-mARNT (WT, mutants, or empty plasmid), 250 ng of XRE reporter, and 2 ng of pRL with 1.2 μl jetPEI for each well. The medium was refreshed with dimethyl sulfoxide (DMSO) or 10 nM TCDD after overnight transfection, luciferase activity was measured another 24 h later using the Dual-Glo luciferase assay system (Promega E2920), and data were normalized by the relative ratio of firefly and *Renilla* luciferase activity.

Coimmunoprecipitation. HEK293T cells were seeded in 10-cm dishes and 2 days later transfected by using 2 μg pCMV-Tag4-mAHR (WT or mutants) and 6 μg pCMV-Tag1-mARNT (WT or mutants) with 16 μl jetPRIME reagent (Polyplus transfection), following the manufacturer's protocol. After overnight incubation, medium was refreshed with DMSO or 10 nM TCDD. Twenty-four hours later, the cells were harvested and shortly sonicated in 500 μl lysis buffer (1× Tris-buffered saline [TBS] with 1 mM EDTA, 1% Triton X-100, and 1× protease inhibitor cocktail [Roche 13744100]) before 10 min of spinning at 12,000 ×*g*. The protein concentration in the supernatant was measured using the Bio-Rad protein assay kit (500-0002). For each sample, 40 μg of supernatant was saved as input for Western blots using the monoclonal antibody [MAb] anti-Flag M2 (F1804, 1:1,000 dilution; Sigma) or c-Myc antibody (9E10, sc-40 horseradish peroxidase [HRP], 1:400 dilution; Santa Cruz Biotechnology). Each immunoprecipitation was performed with 1 mg of supernatant (diluted to 1 ml with lysis buffer) and 40 μl of anti-Flag M2 affinity gel suspension (A2220; Sigma), according to the manufacturer's instructions. Precipitated samples were eluted with 20 μl SDS-PAGE loading buffer and then tested by Western blotting using anti-Myc rabbit MAb (2278, 1:1,000 dilution; Cell Signaling).

Protein data accession number. The atomic coordinates and diffraction data obtained in this work have been deposited in the RCSB Protein Data Bank under accession code 4M4X.

RESULTS

Overall structure of AHR PAS-A domain and its relationship to other PAS domains. The mouse AHR PAS-A domain protein (residues 110 to 267) (Fig. 1A) was obtained using recombinant *E. coli* expression, and crystals were generated that diffracted to a 2.55-Å resolution. We solved the structure using molecular re-

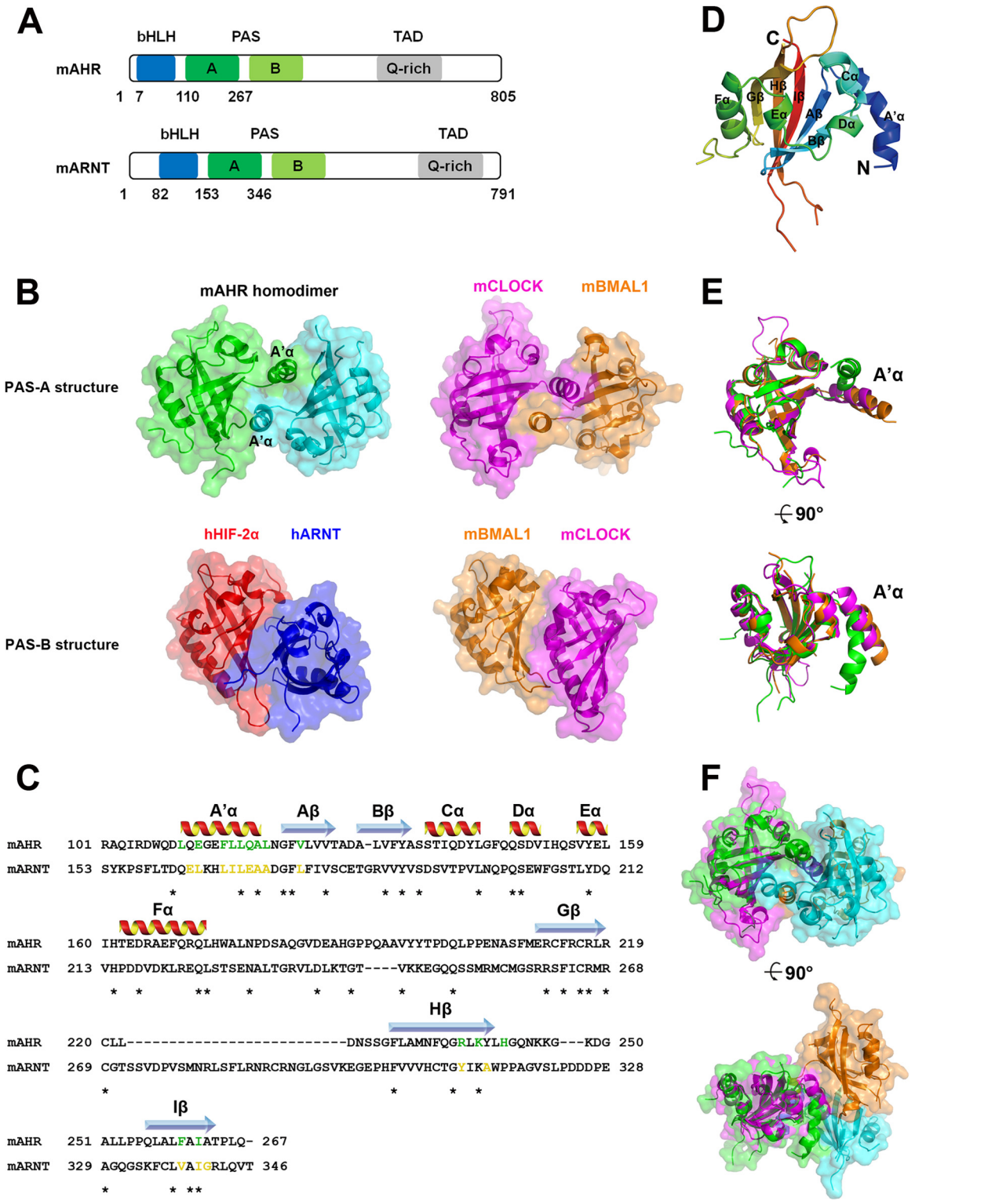

FIG 1 The overall structure of the mouse AHR PAS-A domain. (A) Schematic representation of domain compositions of the AHR and ARNT proteins. (B) Comparison of dimer interfaces of PAS-A and PAS-B domains from bHLH-PAS proteins. The AHR PAS-A domain dimer has an A′α-helix-swapped interface, similar to that of the mouse CLOCK:BMAL1 PAS-A dimer (21). The human HIF-2α:ARNT PAS-B dimer exhibits an antiparallel β-sheet interface (19), while the mouse CLOCK:BMAL1 PAS-B domains dimerize in a roughly parallel fashion (21). (C) Sequence alignment of PAS-A domains of mouse AHR and ARNT. Secondary structure elements are labeled above the alignment, and conserved residues are indicated by asterisks. AHR residues mutated in the functional studies are highlighted in green, and those ARNT residues that may be involved in heterodimer interaction are colored in yellow. (D) Three-dimensional structure of the AHR PAS-A domain with secondary structure elements labeled from N-terminal A′α to the canonical PAS fold in an alphabetical progression, with color ramped from blue to red. (E) Superimposition of PAS fold regions of AHR (green), CLOCK (magenta), and BMAL1 (orange) shows different orientations of the N-terminal A′α-helices. (F) Comparison of the AHR homodimer structure with that of the CLOCK:BMAL1 PAS-A dimer by superimposing one monomer of AHR with CLOCK.

TABLE 1 Data collection and refinement statistics[a]

Parameter	Value(s) for mAHR PAS-A[b]
Data collection	
Space group	P41212
Cell dimensions	
a, *b*, *c* (Å)	88.17, 88.17, 110.01
α, β, γ (°)	90, 90, 90
Resolution (Å)	68.8–2.55 (2.59–2.55)
R_{merge}	0.070 (0.837)
$I/\sigma I$	31.83 (2.54)
Completeness (%)	99.57 (99.30)
Redundancy	9.1 (8.1)
Refinement	
Resolution (Å)	33.9–2.55 (2.64–2.55)
No. of reflections	14,635 (1,415)
R_{work}/R_{free} (%)	20.04/24.46
No. of atoms	
Protein	1910
Water	39
B factors	
Protein	61.1
Water	52.0
RMS deviations[c]	
Bond lengths (Å)	0.006
Bond angles (°)	1.10
Ramachandran statistics	
Favored (%)	97
Outliers (%)	0

[a] The data were obtained from a single crystal.
[b] Values in parentheses are for the highest-resolution shell.
[c] Root mean square deviations.

placement with a combined template consisting of three PAS-A structures, one derived from the *Bacillus subtilis* histidine protein kinase KinA (27) and two from the *Drosophila* PER protein (28, 29). The data collection and refinement statistics are summarized in Table 1. The crystal asymmetric unit contained two AHR molecules arranged as a homodimer, as shown in Fig. 1B. Consistent with the expected PAS fold (1), the AHR PAS-A subunit forms a five-stranded antiparallel β-sheet with the topological strand order B-A-I-H-G, with four accompanying α-helices (Cα, Dα, Eα, and Fα) flanking one side of the β-sheet (see Fig. 1C and D).

Located along the N terminus of the AHR PAS-A domain, a key α-helical structure (denoted as A′α) corresponding to residues 110 to 119 is seen to form a helix-swapped dimer interface with its counterpart from the second subunit (Fig. 1B and C). In addition to the helix-helix interaction, this A′α-helix also interacts across the dimer interface with a portion of the β-sheet from the second subunit. The CLOCK:BMAL1 (21) PAS-A dimer shown in Fig. 1B utilizes a similar overall type of interaction involving the swapped A′α-helices as the central bridging unit. A closer look at these two related PAS-A dimers reveals that the orientation of the A′α-helix of the AHR is slightly different from that seen in the CLOCK:BMAL1 complex (Fig. 1E). The seemingly looser interactions in the CLOCK:BMAL1 dimer interface may be due to an adjustment in that interface required for accommodating the adjacent bHLH and PAS-B dimer interfaces in the same heterodimer (Fig. 1F).

We find that PAS-B dimer interfaces, such as those from HIF-2α:ARNT (19) and CLOCK:BMAL1 (21) complexes, are quite distinct from the PAS-A dimer interfaces we describe here for AHR and that are seen with the CLOCK:BMAL1 heterodimer, as displayed in Fig. 1B. Mammalian PAS-B domains dimerize in a variety of distinct fashions using different interfaces, and these variations may allow these domains to accommodate the other physical and functional requirements of their full-length polypeptides, in some cases also allowing these domains to bind to other types of proteins or small-molecule ligands (2).

Functional importance of the N-terminal A′α-helix. We had not anticipated that the AHR PAS-A domain would show a homodimeric form in the crystal, since full-length AHR had not been previously observed as a functional homodimer (1, 22, 33). Therefore, we explored the possibility that homodimerization of the AHR PAS-A domain is due simply to crystal packing. To study its oligomeric state, we analyzed the solution size of this protein using gel filtration chromatography (Fig. 2A). The mAHR PAS-A protein (residues 110 to 267, WT) has a calculated molecular mass of 21 kDa including the His tag yet shows a single peak with a retention volume of 87.0 ml (corresponding to a size of 37 kDa, approximately) when loaded on the column at a concentration of 120 μM, indicating that it behaves entirely as a homodimer in solution. Furthermore, several diluted samples with concentrations of 80 μM, 16 μM, and 8 μM all displayed similarly positioned gel filtration peaks, as shown in Fig. 2A. This finding suggests that even at a protein concentration as low as 8 μM, the AHR PAS-A domain behaves as a dimer in solution.

The close relationship of the AHR dimer interface in our crystal structure, with the CLOCK:BMAL1 dimer interface previously reported, further supports the notion that the structurally observed arrangement in our crystals is not simply an artifact of crystal packing. To further test whether the A′α-helix-connected dimer interface is important for homodimer formation, as suggested by the crystal structure, we recombinantly produced and purified a ΔA′α mutant (mAHR 120–167, molecular weight of nearly 20 kDa with the His tag) and found this protein to elute with a gel filtration retention volume of 98.1 ml (corresponding to about 17 kDa size). This finding confirms that without the A′α-helix acting as the critical dimerization component, the AHR PAS-A domain will behave as a monomer.

Next, to examine whether the A′α-helix is also important for the transcriptional activity of the AHR full-length protein, we used the XRE luciferase reporter assay shown in Fig. 2B. A deletion of the A′α-helix from the full-length AHR protein caused a dramatic decrease in the transcriptional activity of this mutant (ΔA′α) compared with that of WT AHR in both the absence and presence of the small-molecule ligand TCDD. This finding was consistent when using both AHR-deficient murine hepatoma Tao cells and HEK 293T cells (Fig. 2B).

AHR is known to function mainly as a heterodimer with ARNT *in vivo*. Since the A′α-helix appears to be required for the dimerization and the transcriptional activity of AHR, we asked whether a similar dimerization interface would allow the PAS-A elements of AHR and ARNT to interact effectively in a heterodimer. These two proteins also contain bHLH and PAS-B domains, and each of these separate domains can, in principle, give rise to other dimerization junctions in their heterodimer. We cotransfected full-length AHR and ARNT into 293T cells and assessed by co-IP if these proteins could interact efficiently when only the A′α-helix of AHR was deleted (Fig. 2C). Removal of this helix caused a severe loss in the ability of full-length AHR and ARNT to coassociate in cells. This finding suggests that the AHR

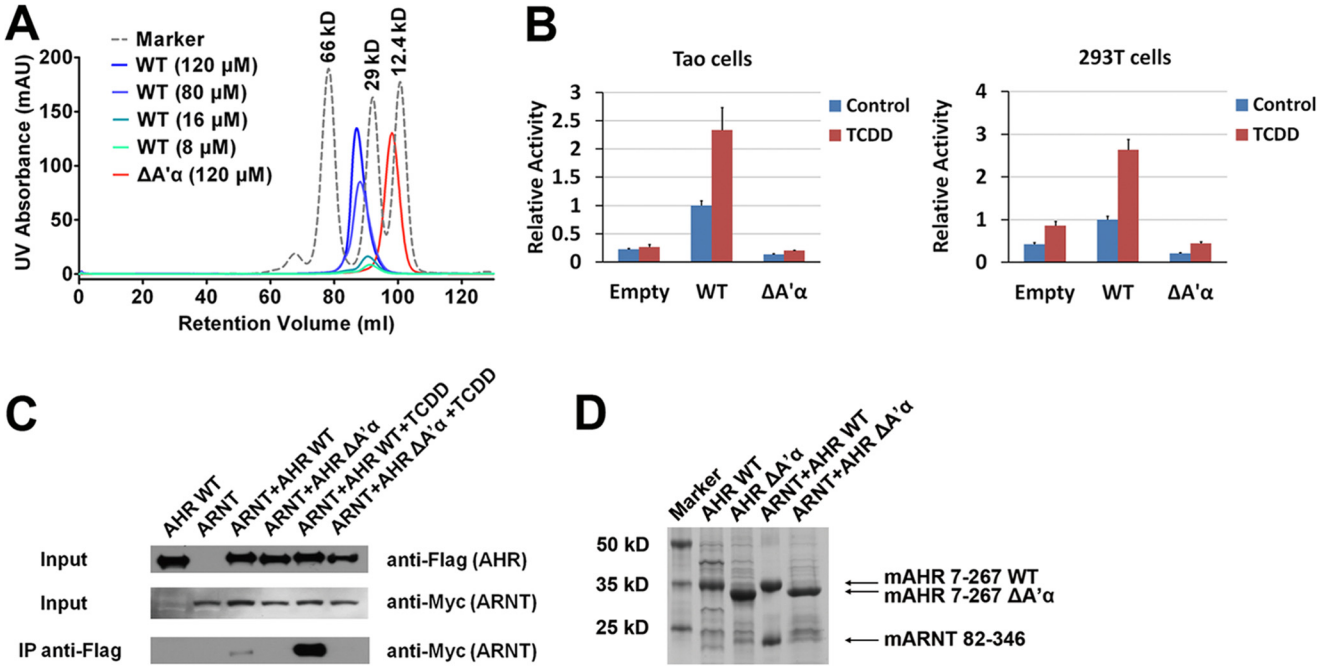

FIG 2 The A′α-helix of the PAS-A domain is essential for AHR dimerization and function. (A) Gel filtration chromatography of the AHR wild-type protein (110 to 267) and the ΔA′α mutant (120 to 267), as well as the marker proteins albumin (66 kDa), carbonic anhydrase (29 kDa), and cytochrome *c* (12.4 kDa). (B) XRE luciferase reporter assay examining the effect of A′α-helix deletion on the transactivation of full-length AHR in both Tao and 293T cells in the presence or absence of ligand TCDD (10 nM). Error bars (SD) are derived from three experiments. (C) Co-IP experiments showing the effects of A′α-helix deletion on association of AHR and ARNT with or without TCDD (10 nM) treatment. (D) Ni affinity pulldown assay assessing the interactions between coexpressed AHR (wild type or ΔA′α mutant) and ARNT proteins, both of which include bHLH and PAS-A domains.

PAS-A homodimerization determinants are also required for AHR:ARNT heterodimerization.

We also tested biochemically the ability of *E. coli* coexpressed AHR and ARNT proteins to associate as a heterodimer in an AHR A′α-helix-dependent manner. Here we used the mAHR 7–267 region and the mARNT 82–346 region, which contain in each case both their bHLH and PAS-A domains (Fig. 1A). As shown in the SDS-PAGE gel of Fig. 2D, ARNT and AHR copurified from a Ni-nitrilotriacetic acid (NTA) column when only AHR contained a His tag (located at its N terminus). The copurification was not possible when the ΔA′α mutant of AHR was used (Fig. 2D). These biochemical findings are fully consistent with our cell-based co-IP results shown in Fig. 2C. Taken together, the transactivation study, the cell-based co-IP study, and the biochemical coassembly experiment all consistently point to the A′α-helix being an essential segment used for AHR's heterodimerization interface with ARNT. While our studies leave open the possibility of PAS-B or bHLH dimerization junctions also being critical in this heterodimer, they do suggest that these other dimerization surfaces, on their own and without the PAS-A interface, are not sufficient to ensure the productive formation of the functional AHR:ARNT heterodimer.

Effect of point mutations at AHR dimerization interface. The interactions at the AHR PAS-A dimer interface involve two distinct regions, both of which involve the participation of the A′α-helix (Fig. 3A). The first region forms between the two reciprocating A′α-helices and consists of hydrophobic interactions between Leu110, Leu117, Ala119, and Leu120. The second one involves the A′α-helix forming contacts with the β-sheet of the other subunit and includes the hydrophobic residues Phe115, Leu116, Ala119 (A′α), Val124 (Aβ), Phe260, Ile262 (Iβ), and a set of polar residues, Ser108, Glu112, Gln118 (A′α), Arg236, Lys238 (Hβ), and His241 (HI loop), as shown in Fig. 3A. Ala119 appears to be critically important, since it is involved in both of these dimerization junctions simultaneously and together with Leu120 maps to the center of the dimer interface (Fig. 3B).

In the previous section, we examined the overall importance of the A′α-helix through its entire deletion. To examine the relative contribution of each specific residue for the dimerization properties of AHR, we made point mutants using mAHR 110 to 267 as the template and analyzed the dimerization abilities of these mutated AHR proteins by gel filtration chromatography profiling (mutants of Phe260 or Ile262 were not included due to their insolubility). As shown in Fig. 4A, all the AHR mutants, except the E112A mutant (85.6 ml), displayed increased retention volumes compared to that of wild-type AHR (87.4 ml). Mutants with a peak position after 91 ml were the F115A (91.4 ml), F115D (91.7 ml), L116E (91.9 ml), A119D (91.8 ml), L120E (91.9 ml), V124D (91.2 ml), F115D/L116E (91.4 ml), and L117E/A119D/L120E (91.3 ml) mutants. Therefore, these point mutations appear to highly disrupt the dimerization ability of AHR, confirming that the crystallographically observed residues, shown in Fig. 3A, are critical for the dimerization of AHR.

We next examined the contribution from each of these interfacial residues in the context of the full-length AHR protein's ability to activate transcription and form heterodimeric interaction with ARNT. For these studies, we employed the XRE reporter assay and the co-IP assay, as described above. We found that mutants carrying the E112A, L116E, A119D, L120E, V124D, F260D, I262D, F115D/L116E, L117E/A119D/L120E,

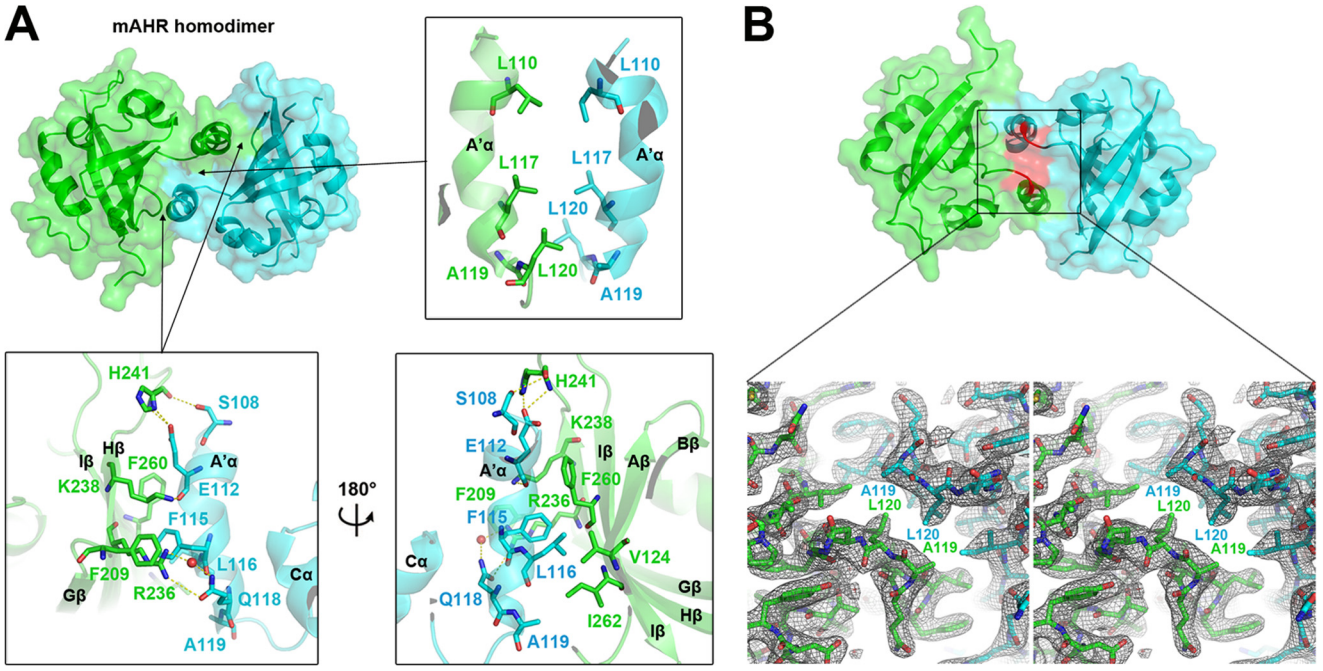

FIG 3 The details of the AHR PAS-A homodimer interface. (A) The interface is composed of two regions: between the two A′α-helices (top) and between one A′α-helix and the β-sheet (bottom). The interfacial residues are labeled and shown in sticks. Hydrogen bonds are indicated as yellow dashed lines, and water molecules are indicated as red dots. The secondary structure elements are labeled. (B) Ala119 and Leu120 locate at the central position of the AHR PAS-A dimer interface. The upper part is 180 degrees rotated from the AHR structure shown in panel A, with Ala119 and Leu120 colored in red. The lower one is a stereo image showing the detailed conformations of Ala119, Leu120, and residues around them in an electron density map (2Fo-Fc map contoured at 1.2 σ).

and V124D/F262D/I262D changes showed luciferase activities that were reduced from that of wild-type AHR in both Tao and 293T cells (Fig. 4B). This loss of activity was correlated with a reduced ability of these AHR mutants to interact physically with the ARNT protein (Fig. 4C). These results together point to a set of six hydrophobic residues in AHR: Leu116, Ala119, Leu120 (A′α), Val124 (Aβ), Phe260, and Ile262 (Iβ), being required for maintaining the overall integrity of the AHR:ARNT heterodimer and its transcriptional activity (Fig. 3A).

Near the C terminus of A′α-helix of AHR, besides Leu116, Ala119, and Leu120, there are two other hydrophobic residues, Phe115 (corresponding to Leu113 of CLOCK or Leu150 of BMAL1) (21) and Leu117, also involved in dimerization (Fig. 3A). But single mutations of these two residues could not totally abolish the transactivation and dimerization properties of AHR:ARNT (Fig. 4) or CLOCK:BMAL1 (21), suggesting that they may not be as significant contributors to heterodimerization as the other six residues identified above.

Dimerization determinants for the PAS-A domains of mammalian bHLH-PAS proteins. The above mutational studies strongly suggest that the amino acid determinants of AHR PAS-A homodimerization are similarly used for heterodimerization with ARNT. To better understand how the AHR:ARNT interface is likely to form through their PAS-A domains in a manner that is also consistent with our mutational data, we built a homology model of the mouse ARNT PAS-A domain by using the SWISS-MODEL server (34) with the BMAL1 structure (21) as the template. We then docked this ARNT PAS-A model in a position identical to that of one of the two AHR subunits in our crystal structure. As shown in Fig. 5A, all six AHR residues confirmed mutationally are able to mediate similar productive interactions with their amino acid counterparts in ARNT. The six reciprocal residues in ARNT (Ile168, Ala171, Ala172, Leu176, Val338, and Ile340; see Fig. 1C) are similarly hydrophobic and are well positioned to form stabilizing contacts in a way similar to that seen in the AHR homodimer (Fig. 5A). This model of AHR-ARNT interactions uses equivalent PAS-A regions in these two proteins for dimerization, as proposed by Hao et al. (22).

The model of AHR:ARNT we constructed also provides a useful template for interpreting the mutational data previously described by others. For example, we found that mutation of AHR residue Glu112 showed an effect on dimerization very similar to that of a mutation on ARNT residue Glu163 (22) (Fig. 1C). Both mutations disrupt heterodimerization, while leading in each case to preferential homodimer formation (22) (Fig. 4), suggesting they may be involved in determining specificity of dimerization. Another mutation, G341D, was reported to be responsible for the defective function of ARNT in Hepa-1 c4 cells (35). In our model (Fig. 5A), Gly341 locates near the end of the Iβ-strand, and its substitution by aspartate would suggest a marked reduction in the stability of the β-sheet and a further loss of dimerization by misorienting Ile340. Ile340 corresponds to Ile262 of AHR (Fig. 4) and Ile317 of BMAL1 (21), both of which have been shown to be critical for dimerization. The two-hybrid study by Hao et al. also identified the ARNT mutation A339D (22) (it locates between two interface residues, Val338 and Ile340, in our model) to be critical for the heterodimerization of ARNT and AHR and for their transcriptional activity. In contrast, the mutation I340V, which modestly changes the hydrophobic side chain, only slightly weakens

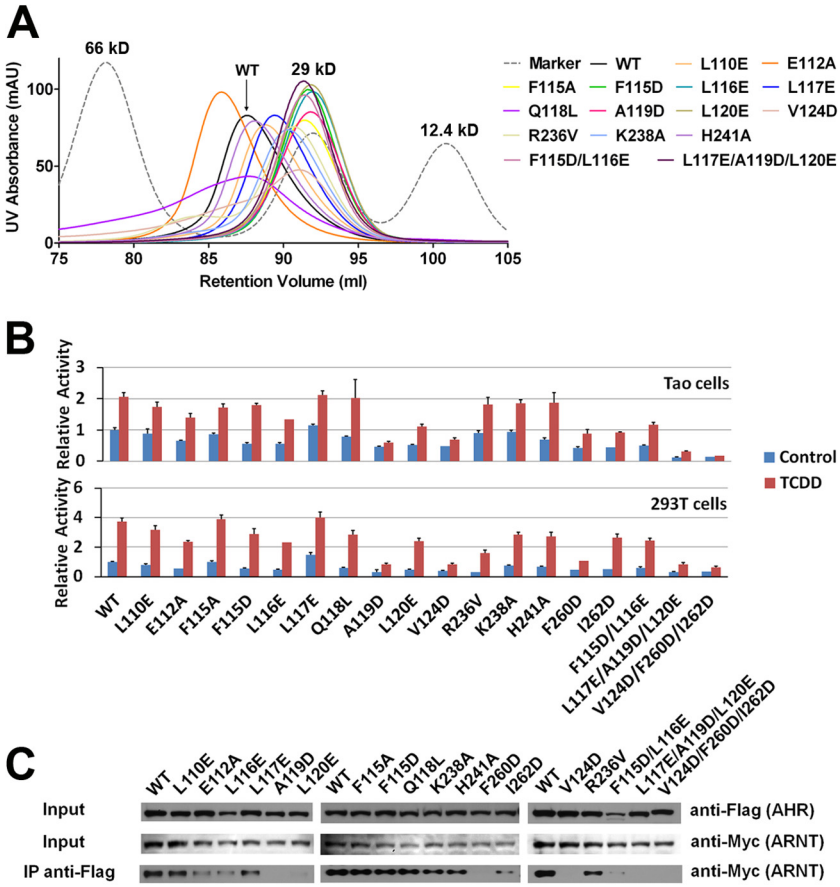

FIG 4 Identification of the contact residues important for dimerization and function of AHR. (A) Gel filtration chromatography of wild-type (WT) and mutated mAHR 110–267 proteins. The same column and protein markers are used as in Fig. 2A. (B) XRE luciferase reporter assay evaluating the effects of mutations on transactivation of full-length AHR in both Tao and 293T cells, with or without TCDD (10 nM) treatment. All error bars (SD) are derived from three samples. (C) Co-IP experiments showing the effects of mutations on the interaction between AHR and ARNT promoted by TCDD (10 nM).

the heterodimerization of these proteins and does not change their transcriptional activity (22).

To further investigate the importance of the ARNT A′α-helix in the AHR:ARNT PAS-A interface, we selected four hydrophobic residues (Leu167, Ile168, Leu169, and Ala171) at the C terminus of the A′α-helix for mutational studies. As shown by the XRE reporter assay in Fig. 5B, the luciferase activities of three full-length ARNT mutants carrying L167E, I168D, and A171D were reduced from that of the wild type in both the absence and presence of TCDD. This finding agrees with results of the co-IP experiment we also carried out, which showed total lost or weakened interactions between AHR and these ARNT mutants (Fig. 5C). These studies highlight the importance of Leu167, Ile168, and Ala171 in mediating the transactivation and dimerization of the AHR:ARNT complex. Interestingly, the other ARNT mutation, L169E, decreased neither the XRE luciferase activity nor the binding to AHR (Fig. 5B and C), similar to the corresponding AHR mutation L117E (Fig. 4B and C). We find that all of our experimental data, as well as the data from the previous published studies, correlate well with the AHR:ARNT PAS-A dimer model shown in Fig. 5A, suggesting its validity.

We next compared our AHR:ARNT model with the CLOCK:BMAL1 PAS-A complex (21) and noted that the six corresponding interfacial residues in CLOCK (Met114, Ala117, Leu118, Phe122, Val252, and Thr254) and those in BMAL1 (Ile151, Ala154, Ala155, Leu159, Val315, and Ile317) were also involved in the PAS-A heterodimer interface, along with several additional hydrophobic residues (Fig. 5D). Most of these interfacial contact residues locate either near the N terminus of the PAS-A domain (A′α and Aβ) or near its C terminus (Iβ). This manner of residue localization may make it possible to coordinate the dimerization of PAS-A domains with the dimerization requirements of bHLH domains at the immediate N-terminal side, and that of the PAS-B domains at the immediate C-terminal side of the PAS-A domains, in the context of full-length proteins.

To more broadly relate the residues used by the AHR PAS-A domain for dimerization to other mammalian bHLH-PAS proteins, we aligned the set of protein sequences shown in Fig. 5E. The six key hydrophobic residues important for AHR dimerization are not absolutely conserved in this family, but their residue counterparts (colored in red) are still mainly hydrophobic residues. This finding is consistent with our expectation that the amino acid distinctions at these six sites may render different binding affinities for pairwise heterodimerization within this family. Moreover, based on the amino acid sequences at the C terminus of A′α, corresponding to AHR Ala119 and Leu120, these bHLH-PAS proteins can be divided into three groups, which also correspond to the functional subclasses of this family (i.e., Ala-Leu for class I

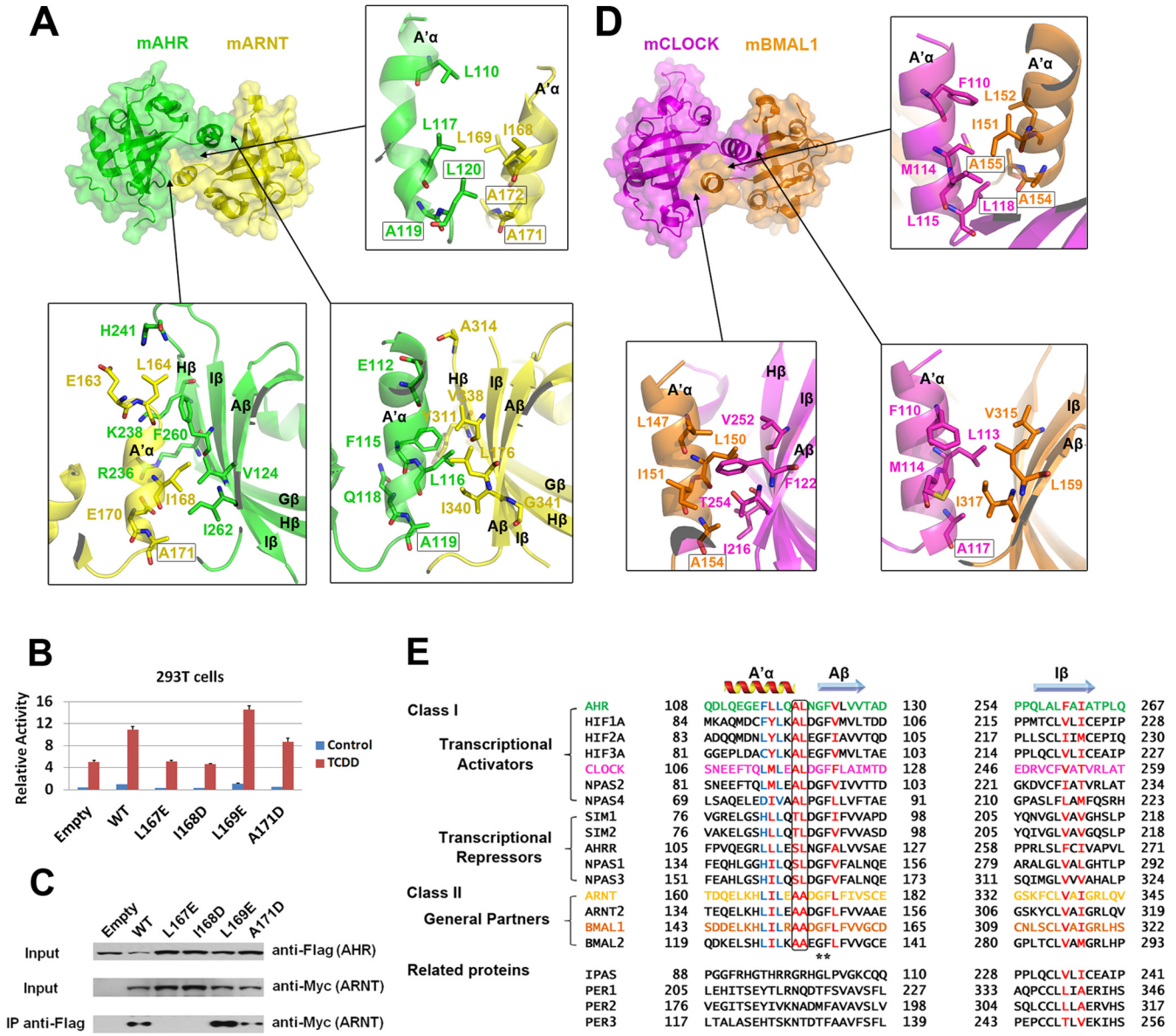

FIG 5 Comparison of PAS-A domains from mouse bHLH-PAS proteins. (A) Homology model of mouse ARNT PAS-A domain forming a heterodimer with AHR. The interactions at the dimer interface are illustrated in three regions: between two A′α-helices (top right), ARNT A′α-helix and AHR β-sheet (bottom left), and AHR A′α-helix and ARNT β-sheet (bottom right). The residues involved in the dimer interface are shown in sticks and annotated. The secondary structure elements are also labeled. (B) Luciferase reporter assay testing the effects of point mutations of full-length ARNT on XRE transactivation in 293T cells, with or without TCDD (10 nM) treatment. (C) Co-IP experiments showing the effects of ARNT mutations on the interaction between AHR and ARNT in the presence of TCDD (10 nM). (D) Reanalysis of mouse CLOCK:BMAL1 PAS-A dimer interface (21) by showing the interactions in three regions: between two A′α-helices (top right), BMAL1 A′α-helix and CLOCK β-sheet (bottom left), and CLOCK A′α-helix and BMAL1 β-sheet (bottom right). Interface residues are shown in sticks and labeled. (E) Multiple sequence alignment of member proteins from the mouse bHLH-PAS family and some related proteins. Only the regions near the N-terminal (A′α-helix and Aβ-strand) or C-terminal (Iβ-strand) regions of the PAS-A domain are aligned. Secondary structure elements are labeled above the alignment, and fully conserved residues are indicated by asterisks. Six hydrophobic residues identified as important for AHR dimerization and their corresponding residues in other bHLH-PAS proteins are colored in red. Residues corresponding to Phe115 and Leu117 of AHR are colored in blue. The central interface residues (counterparts of AHR Ala119 and Leu120) are boxed.

transcriptional activators, [Thr/Ser]-Leu for class I transcriptional repressors, and Ala-Ala for class II general partners) (Fig. 5E). Given the central positions of these two residues at the dimer interface (Fig. 3B), they may be especially important components of partner recognition in this family.

Several related PAS proteins appear to deviate significantly from our suggested model of PAS-A dimerization. The IPAS (inhibitory PAS domain) protein is a spliced variant of HIF-3α, and it dimerizes with HIF-1α but not ARNT (36). We noticed that compared with HIF-3α, IPAS has the same sequence in the bHLH domain and the C-terminal region of the PAS-A domain but a totally changed sequence in the N-terminal region of PAS-A, including the A′α-helix and Aβ-strand (Fig. 5E). Thus, the lack of the A′α-helix could be one reason why IPAS has no ability to bind

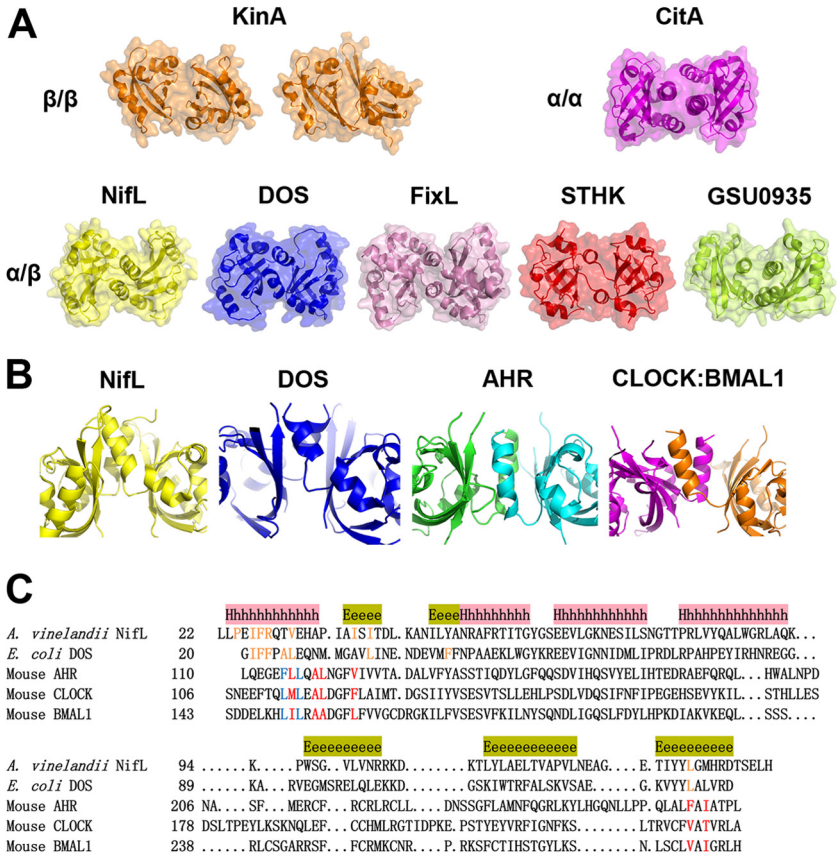

FIG 6 Dimerization properties of PAS-A domains. (A) Three dimerization modes: β-sheet/β-sheet (β/β) mode, represented by *B. subtilis* KinA; α-helix/α-helix (α/α) mode, represented by *K. pneumoniae* CitA; and α-helix/β-sheet (α/β) mode, represented by *A. vinelandii* NifL, *E. coli* DOS, *S. meliloti* FixL, *N. punctiforme* STHK, and *G. sulfurreducens* GSU0935. (B) The orientations and positions of the A′α-helices at the PAS-A dimer interfaces of *A. vinelandii* NifL, *E. coli* DOS, mouse AHR, and mouse CLOCK:BMAL1 complex. (C) Structure-based sequence alignment of NifL, DOS, AHR, CLOCK, and BMAL1 PAS-A domains. The secondary structure elements are indicated above sequences according to that of NifL (α-helix is indicated by "h's," and β-strand is indicated by "e's"). The interface residues of NifL and DOS are colored orange, while those of AHR, CLOCK, and BMAL1 are red or blue, as shown in Fig. 5E.

to ARNT, instead binding to HIF-1α in a presumably unrelated way. Mammalian PERs (PER1, PER2, and PER3) also have tandem PAS domains near the N terminus but have no bHLH domains. The crystal structure of the mouse PER2 fragment (including PAS-A, PAS-B domains, and the αE-helix at the C terminus) revealed a homodimeric interface mediated mainly by the PAS-B β-sheet in an antiparallel orientation, complemented by interactions of the PAS-A domain with PAS-B and the αE-helix (29). Interestingly, in this structure, the short extension N-terminal to the PAS-A domain (corresponding to the A′α-helix region of AHR) does not form a helix but instead forms turns and has an amino acid sequence altogether different from those of the PAS-A domains of the bHLH-PAS family (Fig. 5E). Without the A′α-helix, it is not surprising that PER2 homodimerizes in a dramatically different way from the bHLH-PAS proteins.

DISCUSSION

Based on studies of both mammalian and nonmammalian PAS-A domains, we believe that the formation of homodimers or heterodimers can arise using three modes of interaction. The first mode is represented by the PAS-A domain of *B. subtilis* KinA (27), which forms the dimer interface through two β-sheets (Fig. 6A). Interestingly, in this KinA crystal, there are two types of dimers using the same β-sheet interface while differing in their buried surface areas and packing angles (27). The second dimerization mode requires only α-helices (N- or C-terminal to the core PAS fold) for the interface, as seen in the PAS-A structure of *Klebsiella pneumoniae* sensor histidine kinase CitA (37). The third mode of PAS-A dimerization involves both β-sheets and terminal α-helices. The A′α-helix-swapped interface seen in the PAS-A domains of AHR and the CLOCK:BMAL1 complex (21) is also used by some prokaryotic proteins. For example, PAS-A domains of the nitrogen fixation negative regulator NifL (38) from *Azotobacter vinelandii* and the redox sensor DOS (39) from *E. coli* both form relatively similar interfaces involving A′α-helices and β-sheets (Fig. 6A). However, the positions of their A′α-helices (Fig. 6B) and the sequences of their interface residues (Fig. 6C) are somewhat different from those of AHR and CLOCK:BMAL1. In addition, some prokaryotic proteins with only one PAS domain also use both β-sheets and terminal α-helices to form diverse dimer interfaces, such as those seen with the sensor histidine kinase FixL (40) from *Sinorhizobium meliloti*, the signal transduction histidine kinase STHK (41) from *Nostoc punctiforme*, and the methyl-accepting chemotaxis protein GSU0935 (42) from *Geobacter sulfurreducens* (Fig. 6A).

Except for NPAS2, which binds to heme with both PAS do-

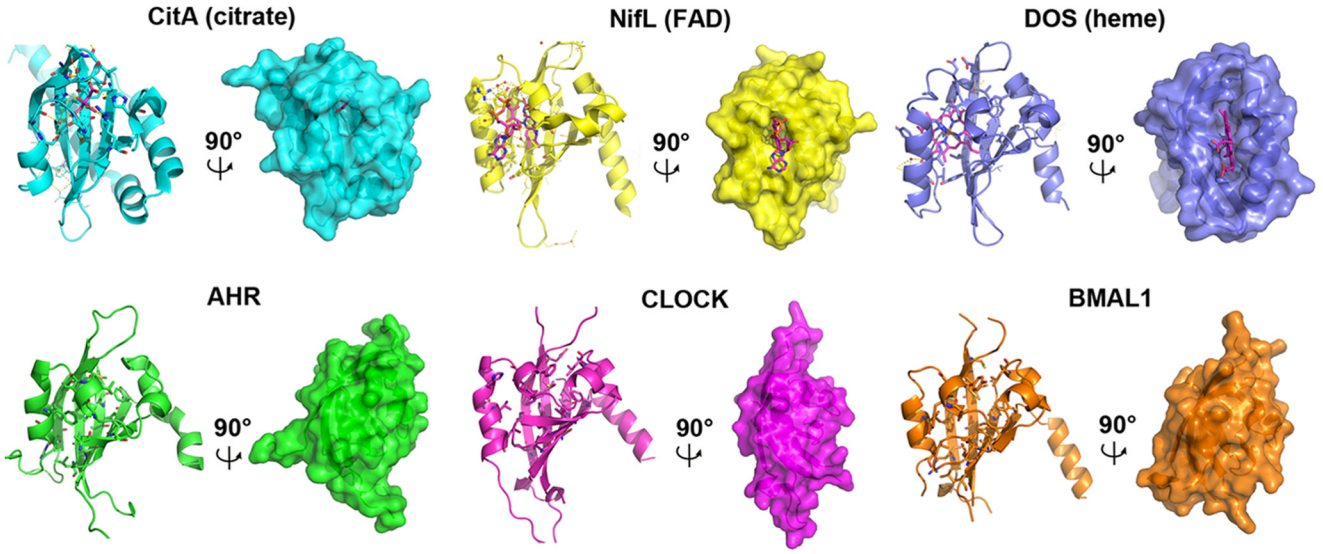

FIG 7 The ligand binding pockets of PAS-A domains. The detailed interactions between ligands (C atoms in magenta) and pocket residues, as well as the clefts on the surfaces, are shown for *K. pneumoniae* CitA (binding citrate), *A. vinelandii* NifL (binding FAD), and *E. coli* DOS (binding heme). For the mouse AHR, CLOCK, and BMAL1 proteins, the residues filling up the pocket positions of PAS-A domains are shown in sticks, and their overall surfaces are also illustrated. The surface view is roughly 90° rotated from the cartoon mode.

mains and functions as a gas-responsive transcription factor (43), the PAS-A domains of most mammalian bHLH-PAS proteins have not been reported to bind small-molecule ligands (2). Meanwhile many other proteins containing multiple PAS domains, such as mouse PER2 (heme) (44) and the prokaryotic proteins CitA (citrate) (37), NifL (FAD) (38), and DOS (heme) (39), use their PAS-A domains for cofactor binding (Fig. 7). Despite the wide diversity of these ligands, the binding pockets of PAS domains are spatially conserved and are formed by the inner surface of the β-sheet and helices Eα and Fα (1) (Fig. 1D). However, in the PAS-A structures of AHR we describe here and in CLOCK and BMAL1 PAS-A domains, this cavity appears to be filled by mainly hydrophobic residues, occluding their surfaces and preventing the binding of hydrophobic ligands (Fig. 7). The PAS-B domain, instead of PAS-A, in AHR has been shown to be the site of binding for small molecules, including TCDD (4, 45).

In summary, we find that PAS-A domains of the mammalian bHLH-PAS proteins AHR:ARNT and CLOCK:BMAL1 dimerize in a similar way, with the A′α-helix-swapped interface mediated mainly by hydrophobic residues. Based on our protein amino acid sequence analysis, we anticipate that other mammalian bHLH-PAS proteins may dimerize in a very similar manner, utilizing similarly positioned amino acids and secondary structure elements within their PAS-A domains. Their distinctions of the two-residue sequence we identify at the C terminus of the A′α-helix for different subclasses, together with other unique residues at their dimeric interface, are likely to be involved in setting their selective patterns of dimerization. Besides the PAS-A domain, the bHLH and PAS-B domains in the family are also expected to participate in the overall heterodimerization patterns of these bHLH-PAS proteins. Other mechanisms controlling the protein level (e.g., oxygen-dependent degradation of HIFs) (2), location (nuclear localization), and timing (negative feedback) further regulate the gene transcriptional activities of bHLH-PAS proteins, probably by controlling their interactions with specific transcriptional coregulators.

ACKNOWLEDGMENTS

We thank Christoph F. Vogel (Department of Environmental Toxicology, UC Davis) for kindly providing us with the murine hepatoma Tao cells and the AHR and XRE reporter plasmids, as well as helpful discussions about the experiments.

REFERENCES

1. **Moglich A, Ayers RA, Moffat K.** 2009. Structure and signaling mechanism of Per-ARNT-Sim domains. Structure **17:**1282–1294.
2. **McIntosh BE, Hogenesch JB, Bradfield CA.** 2010. Mammalian Per-Arnt-Sim proteins in environmental adaptation. Annu. Rev. Physiol. **72:**625–645.
3. **Kewley RJ, Whitelaw ML, Chapman-Smith A.** 2004. The mammalian basic helix-loop-helix/PAS family of transcriptional regulators. Int. J. Biochem. Cell Biol. **36:**189–204.
4. **Denison MS, Soshilov AA, He G, DeGroot DE, Zhao B.** 2011. Exactly the same but different: promiscuity and diversity in the molecular mechanisms of action of the aryl hydrocarbon (dioxin) receptor. Toxicol. Sci. **124:**1–22.
5. **Mimura J, Ema M, Sogawa K, Fujii-Kuriyama Y.** 1999. Identification of a novel mechanism of regulation of Ah (dioxin) receptor function. Genes Dev. **13:**20–25.
6. **Ohtake F, Baba A, Takada I, Okada M, Iwasaki K, Miki H, Takahashi S, Kouzmenko A, Nohara K, Chiba T, Fujii-Kuriyama Y, Kato S.** 2007. Dioxin receptor is a ligand-dependent E3 ubiquitin ligase. Nature **446:**562–566.
7. **Quintana FJ, Basso AS, Iglesias AH, Korn T, Farez MF, Bettelli E, Caccamo M, Oukka M, Weiner HL.** 2008. Control of T(reg) and T(H)17 cell differentiation by the aryl hydrocarbon receptor. Nature **453:**65–71.
8. **Veldhoen M, Hirota K, Westendorf AM, Buer J, Dumoutier L, Renauld JC, Stockinger B.** 2008. The aryl hydrocarbon receptor links TH17-cell-mediated autoimmunity to environmental toxins. Nature **453:**106–109.
9. **Opitz CA, Litzenburger UM, Sahm F, Ott M, Tritschler I, Trump S, Schumacher T, Jestaedt L, Schrenk D, Weller M, Jugold M, Guillemin GJ, Miller CL, Lutz C, Radlwimmer B, Lehmann I, von Deimling A, Wick W, Platten M.** 2011. An endogenous tumour-promoting ligand of the human aryl hydrocarbon receptor. Nature **478:**197–203.
10. **Li Y, Innocentin S, Withers DR, Roberts NA, Gallagher AR, Grigorieva EF, Wilhelm C, Veldhoen M.** 2011. Exogenous stimuli maintain intraepithelial lymphocytes via aryl hydrocarbon receptor activation. Cell **147:**629–640.
11. **Kiss EA, Vonarbourg C, Kopfmann S, Hobeika E, Finke D, Esser C,**

Diefenbach A. 2011. Natural aryl hydrocarbon receptor ligands control organogenesis of intestinal lymphoid follicles. Science **334:**1561–1565.
12. **Ema M, Morita M, Ikawa S, Tanaka M, Matsuda Y, Gotoh O, Saijoh Y, Fujii H, Hamada H, Kikuchi Y, Fujii-Kuriyama Y.** 1996. Two new members of the murine Sim gene family are transcriptional repressors and show different expression patterns during mouse embryogenesis. Mol. Cell. Biol. **16:**5865–5875.
13. **DeBruyne JP, Weaver DR, Reppert SM.** 2007. CLOCK and NPAS2 have overlapping roles in the suprachiasmatic circadian clock. Nat. Neurosci. **10:**543–545.
14. **Teh CH, Lam KK, Loh CC, Loo JM, Yan T, Lim TM.** 2006. Neuronal PAS domain protein 1 is a transcriptional repressor and requires arylhydrocarbon nuclear translocator for its nuclear localization. J. Biol. Chem. **281:**34617–34629.
15. **Sha L, MacIntyre L, Machell JA, Kelly MP, Porteous DJ, Brandon NJ, Muir WJ, Blackwood DH, Watson DG, Clapcote SJ, Pickard BS.** 2012. Transcriptional regulation of neurodevelopmental and metabolic pathways by NPAS3. Mol. Psychiatry **17:**267–279.
16. **Ramamoorthi K, Fropf R, Belfort GM, Fitzmaurice HL, McKinney RM, Neve RL, Otto T, Lin Y.** 2011. Npas4 regulates a transcriptional program in CA3 required for contextual memory formation. Science **334:**1669–1675.
17. **Erbel PJ, Card PB, Karakuzu O, Bruick RK, Gardner KH.** 2003. Structural basis for PAS domain heterodimerization in the basic helix-loop-helix-PAS transcription factor hypoxia-inducible factor. Proc. Natl. Acad. Sci. U. S. A. **100:**15504–15509.
18. **Card PB, Erbel PJ, Gardner KH.** 2005. Structural basis of ARNT PAS-B dimerization: use of a common beta-sheet interface for hetero- and homodimerization. J. Mol. Biol. **353:**664–677.
19. **Scheuermann TH, Tomchick DR, Machius M, Guo Y, Bruick RK, Gardner KH.** 2009. Artificial ligand binding within the HIF2alpha PAS-B domain of the HIF2 transcription factor. Proc. Natl. Acad. Sci. U. S. A. **106:**450–455.
20. **Key J, Scheuermann TH, Anderson PC, Daggett V, Gardner KH.** 2009. Principles of ligand binding within a completely buried cavity in HIF2alpha PAS-B. J. Am. Chem. Soc. **131:**17647–17654.
21. **Huang N, Chelliah Y, Shan Y, Taylor CA, Yoo SH, Partch C, Green CB, Zhang H, Takahashi JS.** 2012. Crystal structure of the heterodimeric CLOCK:BMAL1 transcriptional activator complex. Science **337:**189–194.
22. **Hao N, Whitelaw ML, Shearwin KE, Dodd IB, Chapman-Smith A.** 2011. Identification of residues in the N-terminal PAS domains important for dimerization of Arnt and AhR. Nucleic Acids Res. **39:**3695–3709.
23. **Wu D, Hu T, Zhang L, Chen J, Du J, Ding J, Jiang H, Shen X.** 2008. Residues Asp164 and Glu165 at the substrate entryway function potently in substrate orientation of alanine racemase from E. coli: enzymatic characterization with crystal structure analysis. Protein Sci. **17:**1066–1076.
24. **Minor W, Cymborowski M, Otwinowski Z, Chruszcz M.** 2006. HKL-3000: the integration of data reduction and structure solution—from diffraction images to an initial model in minutes. Acta Crystallogr. D Biol. Crystallogr. **62:**859–866.
25. **McCoy AJ, Grosse-Kunstleve RW, Adams PD, Winn MD, Storoni LC, Read RJ.** 2007. Phaser crystallographic software. J. Appl. Crystallogr. **40:**658–674.
26. **Winn MD, Ballard CC, Cowtan KD, Dodson EJ, Emsley P, Evans PR, Keegan RM, Krissinel EB, Leslie AG, McCoy A, McNicholas SJ, Murshudov GN, Pannu NS, Potterton EA, Powell HR, Read RJ, Vagin A, Wilson KS.** 2011. Overview of the CCP4 suite and current developments. Acta Crystallogr. D Biol. Crystallogr. **67:**235–242.
27. **Lee J, Tomchick DR, Brautigam CA, Machius M, Kort R, Hellingwerf KJ, Gardner KH.** 2008. Changes at the KinA PAS-A dimerization interface influence histidine kinase function. Biochemistry **47:**4051–4064.
28. **King HA, Hoelz A, Crane BR, Young MW.** 2011. Structure of an enclosed dimer formed by the Drosophila period protein. J. Mol. Biol. **413:**561–572.
29. **Hennig S, Strauss HM, Vanselow K, Yildiz O, Schulze S, Arens J, Kramer A, Wolf E.** 2009. Structural and functional analyses of PAS domain interactions of the clock proteins Drosophila PERIOD and mouse PERIOD2. PLoS Biol. **7:**e94. doi:10.1371/journal.pbio.1000094.
30. **Emsley P, Lohkamp B, Scott WG, Cowtan K.** 2010. Features and development of Coot. Acta Crystallogr. D Biol. Crystallogr. **66:**486–501.
31. **Murshudov GN, Vagin AA, Dodson EJ.** 1997. Refinement of macromolecular structures by the maximum-likelihood method. Acta Crystallogr. D Biol. Crystallogr. **53:**240–255.
32. **Adams PD, Afonine PV, Bunkoczi G, Chen VB, Davis IW, Echols N, Headd JJ, Hung LW, Kapral GJ, Grosse-Kunstleve RW, McCoy AJ, Moriarty NW, Oeffner R, Read RJ, Richardson DC, Richardson JS, Terwilliger TC, Zwart PH.** 2010. PHENIX: a comprehensive Python-based system for macromolecular structure solution. Acta Crystallogr. D Biol. Crystallogr. **66:**213–221.
33. **Pongratz I, Antonsson C, Whitelaw ML, Poellinger L.** 1998. Role of the PAS domain in regulation of dimerization and DNA binding specificity of the dioxin receptor. Mol. Cell. Biol. **18:**4079–4088.
34. **Arnold K, Bordoli L, Kopp J, Schwede T.** 2006. The SWISS-MODEL workspace: a web-based environment for protein structure homology modelling. Bioinformatics **22:**195–201.
35. **Numayama-Tsuruta K, Kobayashi A, Sogawa K, Fujii-Kuriyama Y.** 1997. A point mutation responsible for defective function of the arylhydrocarbon-receptor nuclear translocator in mutant Hepa-1c1c7 cells. Eur. J. Biochem. **246:**486–495.
36. **Makino Y, Cao R, Svensson K, Bertilsson G, Asman M, Tanaka H, Cao Y, Berkenstam A, Poellinger L.** 2001. Inhibitory PAS domain protein is a negative regulator of hypoxia-inducible gene expression. Nature **414:**550–554.
37. **Sevvana M, Vijayan V, Zweckstetter M, Reinelt S, Madden DR, Herbst-Irmer R, Sheldrick GM, Bott M, Griesinger C, Becker S.** 2008. A ligand-induced switch in the periplasmic domain of sensor histidine kinase CitA. J. Mol. Biol. **377:**512–523.
38. **Key J, Hefti M, Purcell EB, Moffat K.** 2007. Structure of the redox sensor domain of Azotobacter vinelandii NifL at atomic resolution: signaling, dimerization, and mechanism. Biochemistry **46:**3614–3623.
39. **Kurokawa H, Lee DS, Watanabe M, Sagami I, Mikami B, Raman CS, Shimizu T.** 2004. A redox-controlled molecular switch revealed by the crystal structure of a bacterial heme PAS sensor. J. Biol. Chem. **279:**20186–20193.
40. **Miyatake H, Mukai M, Park SY, Adachi S, Tamura K, Nakamura H, Nakamura K, Tsuchiya T, Iizuka T, Shiro Y.** 2000. Sensory mechanism of oxygen sensor FixL from Rhizobium meliloti: crystallographic, mutagenesis and resonance Raman spectroscopic studies. J. Mol. Biol. **301:**415–431.
41. **Ma X, Sayed N, Baskaran P, Beuve A, van den Akker F.** 2008. PAS-mediated dimerization of soluble guanylyl cyclase revealed by signal transduction histidine kinase domain crystal structure. J. Biol. Chem. **283:**1167–1178.
42. **Pokkuluri PR, Pessanha M, Londer YY, Wood SJ, Duke NE, Wilton R, Catarino T, Salgueiro CA, Schiffer M.** 2008. Structures and solution properties of two novel periplasmic sensor domains with c-type heme from chemotaxis proteins of Geobacter sulfurreducens: implications for signal transduction. J. Mol. Biol. **377:**1498–1517.
43. **Dioum EM, Rutter J, Tuckerman JR, Gonzalez G, Gilles-Gonzalez MA, McKnight SL.** 2002. NPAS2: a gas-responsive transcription factor. Science **298:**2385–2387.
44. **Kitanishi K, Igarashi J, Hayasaka K, Hikage N, Saiful I, Yamauchi S, Uchida T, Ishimori K, Shimizu T.** 2008. Heme-binding characteristics of the isolated PAS-A domain of mouse Per2, a transcriptional regulatory factor associated with circadian rhythms. Biochemistry **47:**6157–6168.
45. **Fukunaga BN, Probst MR, Reisz-Porszasz S, Hankinson O.** 1995. Identification of functional domains of the aryl hydrocarbon receptor. J. Biol. Chem. **270:**29270–29278.